ACS APPLIED MATERIALS & INTERFACES

www.acsami.org

Research Article

Synthesis and Surface Chemistry of 2D TiVC Solid-Solution MXenes

Sanaz Yazdanparast,* Sina Soltanmohammad, Annika Fash-White, Garritt J. Tucker, and Geoff L. Brennecka

Cite This: *ACS Appl. Mater. Interfaces* 2020, 12, 20129–20137

Read Online

ACCESS | Metrics & More | Article Recommendations | Supporting Information

ABSTRACT: MXenes are emerging two-dimensional (2D) materials for energy-storage applications and supercapacitors. Their surface chemistry, which determines critical properties, varies due to different synthesis conditions. In this work, we synthesized TiVC solid-solution MXenes by two different synthesis methods and investigated their surface functional groups. We performed etching of the TiVAlC MAX phase using two different solutions, a highly concentrated HF (50 wt % ≈ 29 M) and a mixture of LiF and HCl (1.9 M LiF/12 M HCl). Large-scale delamination of $TiVCT_x$ to produce single-flake suspension was achieved by further intercalation of the resultant MXene from LiF/HCl with tetrabutylammonium hydroxide (TBAOH). X-ray diffraction indicates a large interlayer spacing of 2.18 nm for $TiVCT_x$ MXene flakes. To investigate the structural stability and adsorption energy of different functional groups on TiVC MXenes, density functional theory (DFT) calculations were performed and supported with X-ray photoelectron spectroscopy (XPS) measurements. A higher concentration of =O and a lower concentration of −F were achieved on the TiVC synthesized by LiF/HCl, both of which provide a more favorable surface chemistry for energy-storage applications. Our results provide the first systematic study on the effect of synthesis conditions on the surface chemistry of solid-solution TiVC MXenes.

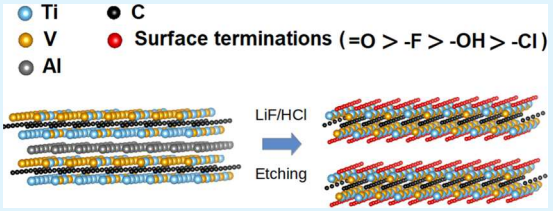

KEYWORDS: *2D MXene, solid-solution TiVC, delamination, surface chemistry, XPS, DFT calculations*

INTRODUCTION

MXenes, a new series of two-dimensional (2D) materials, have attracted great attention due to their unique physical and chemical properties.[1−3] The precursors of MXenes are layered MAX phases with a chemical composition of $M_{n+1}AX_n$, where M is an early transition metal, A is an A-group (mostly group 13 and 14) element, X is C and/or N, and n = 1, 2, or 3.[4,5] Unlike other layered materials such as graphite with weak van der Waals bonding between layers of the multilayer structure, the bonds in the MAX phases are a mixture of metallic, ionic, and covalent bonds.[6] Taking advantage of the different strengths of bonding in the MAX phases—the weak metallic bonding in M−A layers, in particular—the A layer in MAX phases can be removed by aqueous fluorine-containing solutions, resulting in the formation of MXenes and conversion of the three-dimensional (3D) MAX structure to a 2D MXene.[2,5,7,8] The general formula of MXenes is $M_{n+1}X_nT_x$, where T represents surface functional groups (=O, −F, −OH, and/or −Cl) and x is the number of functional groups per formula unit.[9−12] MXenes have been considered for a variety of applications[2,13−16] and, among all of them, their use as electrode materials in energy-storage applications has attracted the most attention.[11,17,18] The surface chemistry, or termination groups, of MXenes significantly affects their electrochemical energy-storage properties.[19−21] For example, it has been reported that =O terminations in MXenes increase the energy-storage capacity, while −F and −OH terminations in MXenes block electrolyte ion transport and subsequently decrease the energy-storage capacity.[22−25] Etching condition has been considered as one of the important methods to affect the surface chemistry of MXenes. However, except one study, which was performed on the effect of etching condition on the surface termination of $Ti_3C_2T_x$ MXenes,[26] no other systematic studies have shown how to tailor surface termination of other MXenes during synthesis.

Depending on the number of M elements and their arrangement in the structure, MXenes can have different structural forms: mono-M elements, solid-solution M elements, and ordered double-M elements.[27] MXenes of solid-solution M elements contain two different transition metals with a random arrangement in the M layers, while MXenes of ordered double-M elements contain single or double layers of only one transition metal sandwiched between layers of a second transition metal.[27,28]

Until now, the large majority of studies have focused on the synthesis and delamination of mono-M element MXenes.[17,29−33] However, it is known that utilizing a combination of elements in the M site, either as solid solutions

Received: February 19, 2020
Accepted: April 3, 2020
Published: April 3, 2020

https://dx.doi.org/10.1021/acsami.0c03181
ACS Appl. Mater. Interfaces 2020, 12, 20129−20137

or in an ordered phase, may provide an effective method to tune the properties of MXenes.[34,35] Synthesis of two solid-solution M_2X-type MXenes has been reported; the stacked $TiNbCT_x$ MXene was synthesized using 50% HF and its delamination was achieved using hydrazine,[10,36] and stacked $TiVCT_x$ MXene was produced recently by a mixture of lithium fluoride salt (LiF) and hydrochloric acid (HCl).[37] It is worth noting that the majority of synthesized MXenes were created using a high concentration of HF in the etching process, which is far from ideal from a safety perspective and also affects the quality, surface chemistry, and properties of the resultant MXenes.[38,39]

Herein, we systematically study the effect of etching conditions on the surface chemistry of $TiVCT_x$ MXenes. We show that large-scale delamination and separation of this type of 2D materials can be achieved by further intercalation of the resultant MXene using tetrabutylammonium hydroxide (TBAOH). In addition, we used density functional theory (DFT) calculations to predict the structural stability and adsorption behavior of different functional groups on TiVC MXenes. X-ray photoelectron spectroscopy (XPS) provides experimental validation of these calculations by measuring the surface chemistry and concentration of functional groups on TiVC MXenes.

MATERIALS AND METHODS

Synthesis of the Solid-Solution TiVAlC MAX Phase. The solid-solution TiVAlC MAX phase was prepared according to the procedure reported by Naguib[40] and Wang *et al.*[37] TiVAlC was synthesized by heating a mixture of titanium, Ti (Alfa Aesar, USA, 99 wt % purity, −325 mesh), vanadium, V (Sigma-Aldrich, USA, 99.5 wt % purity, −325 mesh), aluminum, Al (Alfa Aesar, USA, 99.5 wt % purity, −325 mesh), and graphite, C (Alfa Aesar, USA, 99 wt % purity, −325 mesh) elemental powders in a molar ratio of 1.0:1.0:1.3:1.0 to 1450 °C in argon at 5 °C/min, followed by a 2 h holding period at this temperature. The resultant MAX phase was crushed using a mortar and pestle and sieved through a mesh 325 sieve (particle size ≤ 45 μm).

Synthesis of Solid-Solution $TiVCT_x$ MXenes. $TiVCT_x$ MXene was produced by immersing ∼1 g of the parent MAX phase into a 12 mL solution of hydrochloric acid and lithium fluoride at 55 °C for 60 h. The mixture of LiF/HCl (1.9 M LiF/12 M HCl) was prepared by dissolving 0.6 g of LiF in 12 ml of HCl (37 wt % ≈ 12 M HCl) at RT. After etching, the resultant suspension was washed with deionized water and centrifuged to separate the powders from the supernatant. After several washing procedures and achieving pH ≈ 6, the product was dried at room ambient. In this work, the TiVAlC MAX phase was also treated with 50% HF for 24 h at room temperature to compare its elemental composition with the MXene prepared by LiF/HCl solution.

Delamination of MXenes and Fabrication of MXene Films. $TiVCT_x$ MXenes were delaminated by mixing 0.2 g of stacked MXenes (prepared by LiF/HCl) with 2 ml aqueous solution of 54−56% tetrabutylammonium hydroxide (TBAOH; $(C_4H_9)_4NOH$) at RT for 5 h with magnetic stirring. Then, the resulting mixture was centrifuged at 3500 rpm for 15 min to separate the intercalated MXene from the liquid. The supernatant liquid was decanted, and the intercalated MXene was washed with 10 ml of DI water to remove the remaining TBAOH residue. After decanting the supernatant, 20 mL of DI water was added to the intercalated powder, hand-shaken for 2 min, centrifuged at 3500 rpm for 1 h, and finally stable MXene colloidal suspension was decanted into a glass vial. To fabricate MXene films, a concentrated colloidal suspension of MXenes was drop-casted on a cover glass.

Material Characterization. The crystal structures of the MAX phase and MXenes were characterized by a PANalytical (nee Philips) X-Pert Pro MPD X-ray diffractometer (XRD) using Cu Kα radiation (wavelength 1.54056 Å) at 45 kV and 40 mA. Rietveld refinement was performed using the High Score Plus software package by PANalytical and crystallographic information file (CIF) from ICDD (International Centre for Diffraction Data).[41] The surface morphology and elemental compositions of powders were characterized by scanning electron microscopy (SEM, JSM-7000F) equipped with "Octane Pro" SDD energy-dispersive spectroscopy (EDS). The XPS analysis was performed on as-prepared pellets (produced by cold pressing the dried powders at a load corresponding to 1 GPa) using a Scienta Omicron, HiPP-3 Environmental XPS with monochromated Al Kα radiation. The XPS survey spectrum and high-resolution XPS scan spectra were recorded at pass energies of 500 and 200 eV, respectively. Component peak fitting of XPS spectra was performed by using the CasaXPS software.

Density Functional Theory Calculations. DFT calculations were performed to investigate the stability of functionalized TiVC, its functionalization site, and the adsorption energy of various termination groups. Calculations were undertaken using the Vienna *Ab initio* Simulation Package (VASP) code.[42−45] Interaction between the valence electrons and atoms was represented using the projector augmented wave (PAW) method,[46] and the exchange correlation energy between electrons was represented using the Perdew−Burke−Ernzerhof general gradient approximation (PBE) functional.[47] The Methfessel−Paxton method was used to define partial orbital occupation, with a smearing width of 0.1 eV. The energy convergence criterion was 10^{-6} eV, the force convergence criterion was 0.005 eV/Å, and calculations were performed with a 13 × 13 × 1 *k*-point mesh. Single $TiVCT_x$ layers were modeled in a 3D periodic supercell that contained approximately 20−22 Å of vacuum on both sides of the MXene structure to remove self-interaction. All structure energies were calculated following system relaxation, where ion positions were updated using the conjugate gradient method.

RESULTS AND DISCUSSION

XRD Analysis of the Solid-Solution MAX Phase and MXene. XRD patterns of the as-prepared solid-solution TiVAlC MAX phase, its corresponding stacked MXene synthesized by LiF/HCl, and the MXene film on the cover glass are shown in Figure 1. The as-prepared TiVAlC contains Ti_3AlC_2 as an impurity phase (star symbols show Ti_3AlC_2 peaks). The existence of a secondary impurity phase is common in MAX phases.[11,37,39,40] To quantify the amount of

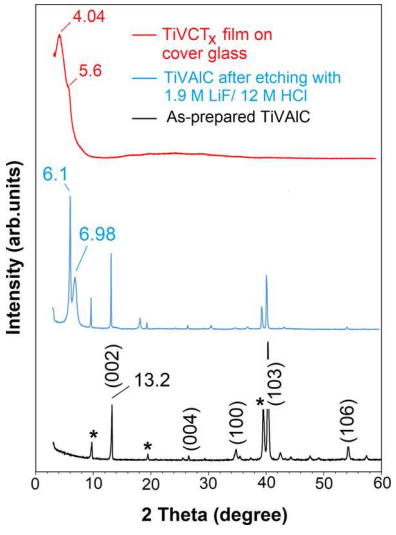

Figure 1. XRD (Cu Kα) patterns of the as-prepared TiVAlC MAX phase, after etching with LiF/HCl and $TiVCT_x$ MXene films on the cover glass; the stars (*) represent peaks of Ti_3AlC_2 that existed as an impurity phase in the TiVAlC MAX phase.

https://dx.doi.org/10.1021/acsami.0c03181
ACS Appl. Mater. Interfaces 2020, 12, 20129−20137

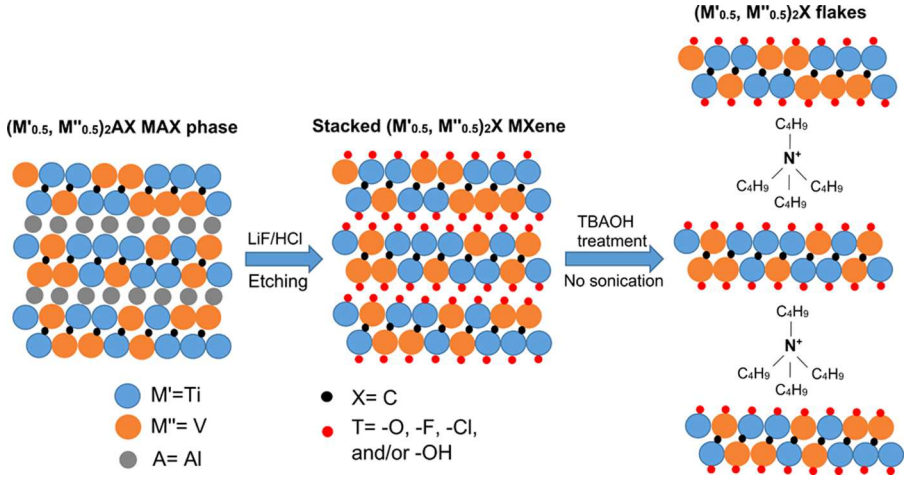

Figure 2. Schematic of the solid-solution TiVC MXene formation by wet chemical etching and its delamination using TBAOH.

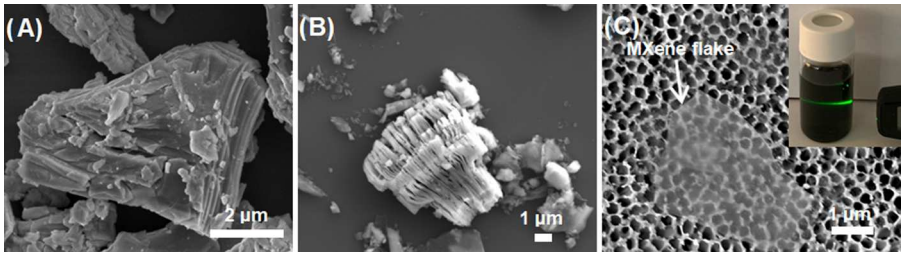

Figure 3. SEM of (A) as-prepared TiVAlC MAX phase, (B) stacked TiVCT$_x$ MXene synthesized by LiF/HCl, and (C) TiVCT$_x$ MXene flake. The inset shows the Tyndall effect in a stable colloidal suspension of MXene in water.

each MAX phase, Rietveld refinement was employed (Figure S1, Supporting Information) using #153266 and #198589 CIF files for Ti_3AlC_2 and TiVAlC phases, respectively. The results indicated the existence of ~69 wt % TiVAlC and ~31 wt % Ti_3AlC_2 in our as-synthesized MAX phase. Based on Rietveld analysis, the calculated lattice constants of Ti_3AlC_2 are a = 3.02 Å and c = 18.21 Å and those of TiVAlC are 2.97 and 13.41 Å. This strongly suggests a Ti/V ratio in TiVAlC of approximately 1 based on Vegard's law and the associated lattice parameters of isostructural end members of Ti_2AlC (a = 3.04 Å, c = 13.60 Å) and V_2AlC (a = 2.91 Å, c = 13.14 Å) according to ICDD No. 29-0095 and 29-0101, respectively.[41] After etching the powder with 1.9 M LiF/12 M HCl solution for 60 h at 55 °C, clay-like sediment was formed with a corresponding shift of the (002) peak to 2θ = 6.10 and 6.98°, indicating the successful formation of the MXene and/or MXenes with different interlayer spacings of 1.44 and 1.26 nm, respectively. Since two different MAX phases are in the as-prepared powder, two MXenes can be formed after etching; the peak at 2θ = 6.98° can be assigned to $Ti_3C_2T_x$,[17] while the peak at 2θ = 6.10° can be related to the formation of TiVCT$_x$. Compared to the synthesized MXene by LiF/HCl, the XRD pattern of the resultant MXene from 50% HF shows a shift of the (002) peak to 2θ = 6.26° corresponding to an interlayer spacing of 1.41 nm (Figure S2A, Supporting Information).

To further study the formation of TiVCT$_x$ MXene, the resultant sediment synthesized by LiF/HCl was treated with TBAOH for 5 h at room temperature, forming a stable colloidal suspension of separated TiVCT$_x$ MXene flakes in water. It is worth noting that delamination of the $Ti_3C_2T_x$ MXene is not possible with large molecules of TBAOH after such a short time.[39] In addition, no green color colloidal suspension, which is an optical evidence of $Ti_3C_2T_x$,[39,48] was observed after treating the MAX phase with the LiF/HCl mixture, suggesting that if $Ti_3C_2T_x$ is formed, its amount is much less than that of the TiVCT$_x$ MXene. After treating the stacked TiVCT$_x$ MXene with TBAOH and drop casting its colloidal suspension on a cover glass, we performed XRD on the film (red plot). A larger shift of the (002) peak can be seen in the deposited film, 2θ = 4.04°, corresponding to a d-spacing of 2.18 nm. The increase in the d-spacing of the deposited film is due to the intercalation of tetrabutylammonium ions (TBA^+) and/or water molecules between MXene flakes.[32,49] A small broad shoulder for the (002) peak is also apparent at 2θ = 5.6°, which can be due to the TBAOH treatment.[32] Only the (002) peak was observed for the TiVCT$_x$ MXene film, indicating fully delaminated MXene flakes lying horizontally on the cover glass.[50]

SEM and EDS Analyses of the Solid-Solution TiVAlC MAX Phase and TiVCT$_x$ MXene. The multilayer solid-solution MXene formation and its delamination are schematically illustrated in Figure 2. The layered MAX phase reacts with LiF/HCl, resulting in the removal of the Al layers to form stacked MXenes. Due to the aqueous etching, the exposed M′M″ atoms (Ti and V) have a high tendency to form bonds with hydrophilic groups such as =O, −F, −OH, and/or −Cl, leading to negatively charged MXene surfaces.[51] Electrostatic attraction between the negatively charged MXene flakes and cations such as Li^+ and TBA^+ (as well as the attraction of water molecules to the hydrophyllic surfaces) results in an increase of interlayer spacing between MXene sheets and separation of MXene flakes from each other.[52,53] Based on the above discussion, the following reactions are assumed during the

https://dx.doi.org/10.1021/acsami.0c03181
ACS Appl. Mater. Interfaces 2020, 12, 20129−20137

Table 1. Elemental Composition (at. %) of the Solid-Solution TiVAlC MAX Phase and $TiVCT_x$ MXenes Prepared by Two Different Solutions. EDS was Obtained from At Least Four Different Particles for Each Sample

sample	Ti	V	Al	C	O	F	Cl	Si
as-prepared TiVAlC	23 ± 4	26 ± 3	28 ± 2	20 ± 6				5 ± 3
TiVAlC after etching with 29 M HF	17 ± 3	12 ± 3	3 ± 2	34 ± 7	15 ± 4	18 ± 2		
TiVAlC after etching with 1.9 M LiF/12 M HCl (stacked layer)	16 ± 1	20 ± 1	1 ± 0.2	20 ± 1	24 ± 1	6 ± 1	8 ± 1	4 ± 1

exfoliation process of the solid-solution TiVAlC MAX phase in the mixture of LiF and HCl solutions[5,54]

$$TiVAlC + 6HCl + 6\,LiF = TiVC + Li_3AlF_6 + AlCl_3 + 3\,LiCl + 3H_2\uparrow \quad (1)$$

$$TiVC + 2H_2O = TiVC(OH)_2 + H_2\uparrow \quad (2)$$

$$TiVC + 2H_2O = TiVCO_2 + 2H_2\uparrow \quad (3)$$

$$TiVC + 2\,HCl = TiVCCl_2 + H_2\uparrow \quad (4)$$

$$TiVC + 2\,HF = TiVCF_2 + H_2\uparrow \quad (5)$$

Reaction 1 shows the removal of the Al layer from the MAX phase, and Reactions 2−5 show the formation of MXene with different possible surface functional groups.

Scanning electron microscopy (SEM) images of the as-prepared MAX phase, its corresponding stacked MXene, and the delaminated flakes are shown in Figure 3. The compact layered structure of the MAX phase can be seen in Figure 3A. After etching the MAX phase with a mixture of HCl and LiF, the Al layers are removed, resulting in the exfoliation of TiVC layers (Figure 3B). A similar result has been observed for the TiVC layers synthesized by 50% HF (Figure S2B, Supporting Information). Large-scale delamination and separation of solid-solution TiVC MXene layers are achieved by intercalation of the resultant stacked MXene synthesized by LiF/HCl with TBAOH at RT for 5 h. Delaminated MXene flakes were dispersed in DI water to form a stable colloidal suspension, which is confirmed by the Tyndall effect (the inset in Figure 3C). Figure 3C shows $TiVCT_x$ MXene flakes after drop casting the colloidal suspension on an alumina membrane.

To confirm the formation of the solid-solution MXene and analyze its elemental composition, the resultant sediments prepared by two different solutions (HF and LiF/HCl) were analyzed by energy-dispersive X-ray spectroscopy (EDS) (Table 1). All of the powders were placed on Si wafers as a substrate, resulting in a silicon signal for most samples. As shown in Table 1, the Al content was significantly reduced after etching the MAX phase powder by both LiF/HCl and concentrated HF, confirming the formation of $TiVCT_x$ MXene. Various surface terminations such as =O, −F, and −Cl were detected by EDS for MXenes produced by the LiF/HCl solution. For $TiVCT_x$ MXene produced by 29 M HF, a large amount of −F is observed. Comparing the EDS results of stacked MXenes prepared by two different etchant solutions, the amount of −F termination was reduced in the synthesized MXenes by 1.9 M LiF/12 M HCl, which has been reported as favorable for energy-storage applications.[21−25]

DFT Calculations of Structural Stability and Adhesion Behavior of Functional Groups on TiVC MXene. To predict the structural stability of the functionalized $TiVCT_x$ MXene and the adsorption energies of the different termination groups, DFT calculations were performed. Three base structures with different transition-metal ion configurations were used to represent the solid-solution TiVC MXene (Figure S3, Supporting Information). Figure 4 shows

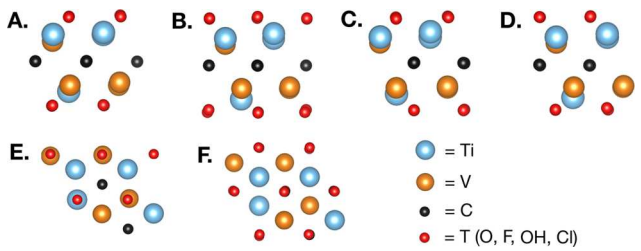

Figure 4. Functionalized MXene with different configurations of possible termination groups studied in the DFT calculations. Two metastable adsorption sites are assumed on MXene surfaces. (A−D) Side views of these configurations, where the structures in (A) and (B) have the same sites on each layer, while the structures in (C) and (D) have different sites. MXene structures shown in (E) and (F) show the top view of the two functional sites of (A) and (B), respectively.

the functionalized MXene with different configurations of termination groups adsorbed to the base structures. Four different termination sites were considered: two with symmetric functionalization (A and B structures in Figure 4) and two with different functional sites on either side of the layer (C and D structures in Figure 4). These configurations were chosen based on the metastable MXene termination sites reported by Khazaei et al.[55] The configuration referred to as A, in which the functional group is adsorbed above the opposite-side transition-metal ion, had the lowest total energy, cohesive energy, and adsorption energy among the four possible termination configurations studied here.

To calculate the structural stability of the functionalized TiVC MXene, the cohesive energy per atom was calculated (eq 6). The cohesive energy per atom is the energy of each individual atom in the MXene isolated in a vacuum subtracted from the total energy of the MXene structure, normalized by the number of atoms, indicating the energetic cost of splitting the MXene structure into its constituent elements.

$$E_{coh/atom} = [E_{tot}(TiVCT_x) - E_{atom}(Ti) - E_{atom}(V) - E_{atom}(C) - 2E_{atom}(O/F/Cl/H)]/n \quad (6)$$

where n is the number of atoms, E_{tot} is the total energy of $TiVCT_x$, and E_{atom} is the energy of individual atoms in a vacuum.

The calculated cohesive energies are shown in Table S1 (Supporting Information) and Figure 5A for $TiVCT_2$ MXenes. These results show that $TiVCT_2$ MXenes with the =O termination group possess the lowest cohesive energy compared to −F, −OH, and −Cl terminations, suggesting that $TiVCO_2$ MXene is the most energetically stable $TiVCT_2$ MXene structure in this study.

To investigate TiVC's relative preference for adsorbing the four possible termination groups, the adsorption energy of

https://dx.doi.org/10.1021/acsami.0c03181
ACS Appl. Mater. Interfaces 2020, 12, 20129−20137

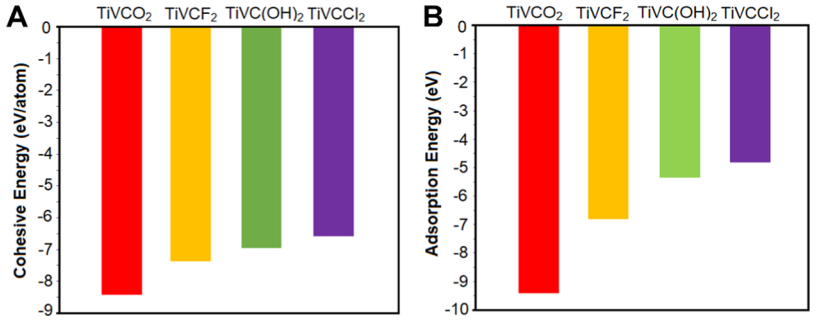

Figure 5. Calculated (A) cohesive energies and (B) adsorption energies for various functionalized TiVC MXenes using DFT.

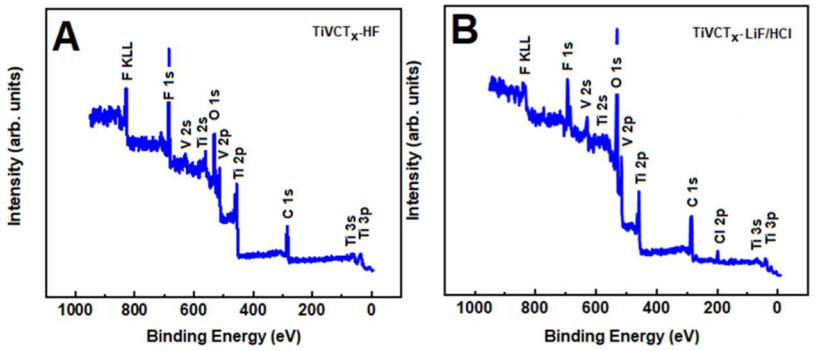

Figure 6. XPS spectra of TiVCT$_x$ MXenes synthesized by (A) 50% HF and (B) LiF/HCl. XPS confirmed the removal of Al and formation of TiVCT$_x$ MXenes with different functional groups.

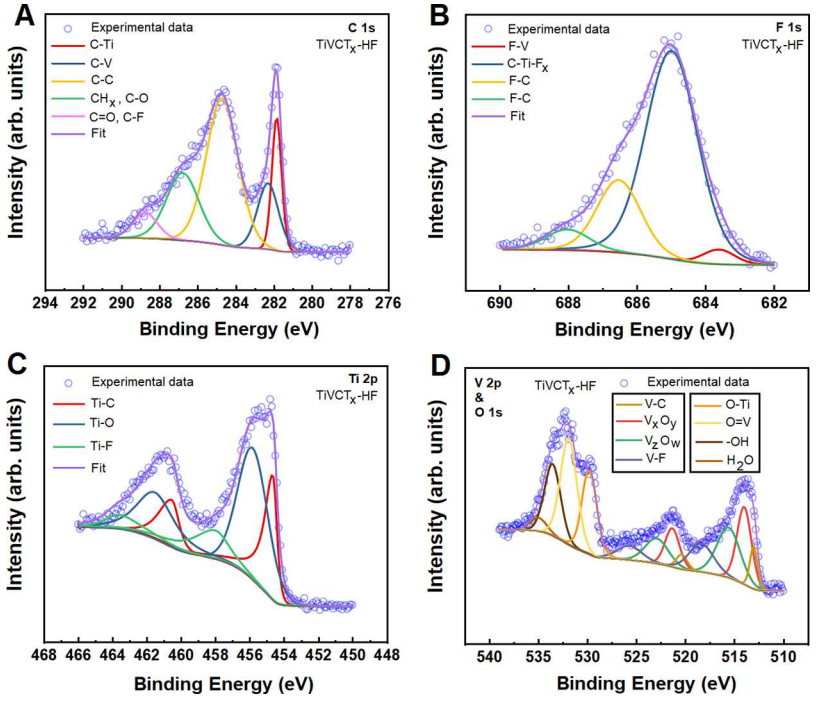

Figure 7. High-resolution XPS spectra of TiVCT$_x$-HF MXene in (A) C 1s, (B) F 1s, (C) Ti 2p, and (D) V 2p and O 1s regions. See the text for discussion.

each termination group was calculated. Adsorption energy has been used to predict the most favored termination group in many other MXenes.[9,55] The adsorption energy of different termination groups at the surface of TiVC MXene was calculated by subtracting the energy of the pristine MXene and the energy of the isolated termination group atoms in a vacuum (O, F, OH, or Cl) from the total energy of the functionalized MXene, as defined in eq 7.

$$E_{ads} = \frac{E_{tot}(\mathrm{TiVCT}_x) - E(\mathrm{TiVC}) - 2E(\mathrm{T}_x)}{2} \quad (7)$$

where E_{tot} is the total energy of the functionalized MXene, $E(\mathrm{TiVC})$ is the total energy of the pristine MXene, and $E(\mathrm{T}_x)$

https://dx.doi.org/10.1021/acsami.0c03181
ACS Appl. Mater. Interfaces 2020, 12, 20129−20137

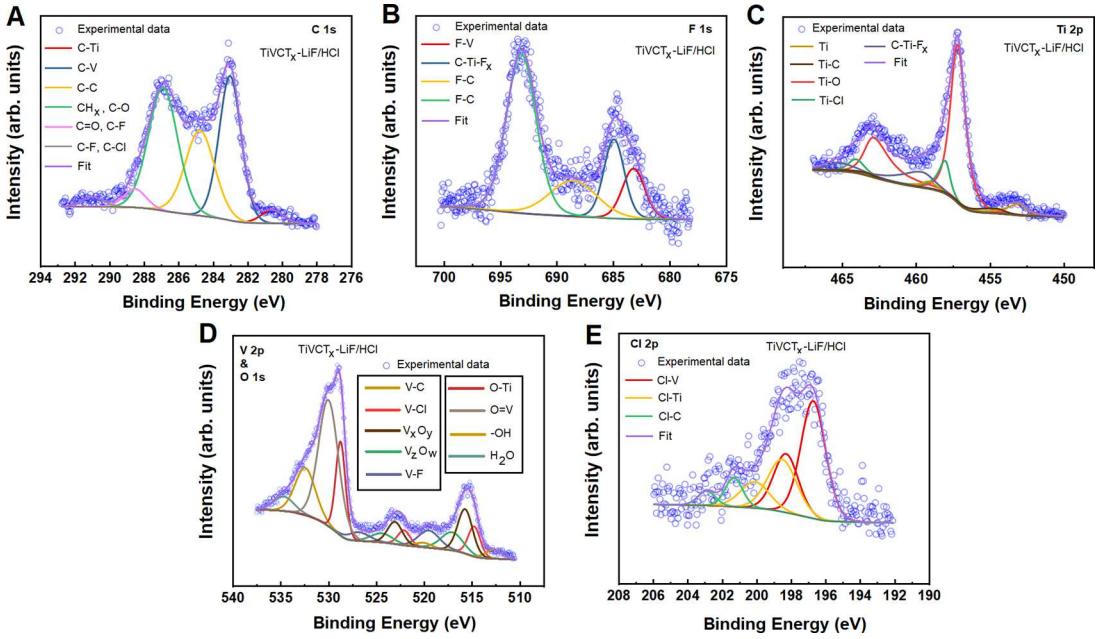

Figure 8. High-resolution XPS spectra of $TiVCT_x$-LiF/HCl MXene in (A) C 1s, (B) F 1s, (C) Ti 2p, (D) V 2p and O 1s, and (E) Cl 2p regions. See the text for discussion.

Table 2. Surface Composition (at. %) of $TiVCT_x$ MXenes Measured by XPS

sample	Ti	V	C	O	F	Cl
$TiVCT_x$-HF	9.6 ± 0.2	7.9 ± 0.16	39.7 ± 0.51	22.9 ± 0.43	19.9 ± 0.33	
$TiVCT_x$-LiF/HCl	4.6 ± 0.15	6.5 ± 0.12	40.1 ± 0.54	34.1 ± 0.5	11.6 ± 0.34	3.1 ± 0.23

is the total energy of the isolated functional group atoms in a vacuum. The results of adsorption energies are presented in Table S2 (Supporting Information) and Figure 5B. It is shown that TiVC with the =O termination group has the lowest value of adsorption energy, followed by −F, −OH, and −Cl termination groups.

XPS Analysis of $TiVCT_x$ MXene. To support our DFT calculations and analyze the surface chemistry of the synthesized TiVC MXene, XPS measurements were performed. The survey spectra of $TiVCT_x$-HF and $TiVCT_x$-LiF/HCl (Figure 6) show that Al was removed from the MAX phase and $TiVCT_x$ MXene was formed. Oxygen and fluorine functional groups were clearly observed in the XPS results of both $TiVCT_x$-HF and $TiVCT_x$-LiF/HCl. In addition, the presence of chloride (−Cl) is shown in the $TiVCT_x$-LiF/HCl sample (Figure 6B).

Figures 7 and 8 show high-resolution XPS spectra and peak fitting of different regions in $TiVCT_x$-HF and $TiVCT_x$-LiF/HCl samples. The peak positions obtained from the fits are listed in Tables S3 and S4 (Supporting Information).

In the C 1s region of $TiVCT_x$-HF (Figure 7A), the spectrum is fitted by five peaks. The first two peaks at 281.8 and 282.3 eV correspond to internal C−Ti and C−V bonds.[56,57] Three other peaks are assigned to graphitic C−C (285 eV), C−O/C−H (286.8 eV), and C=O and/or C−F (288.7 eV) bonds.[56,58−61] The C 1s region for the $TiVCT_x$-LiF/HCl sample (Figure 8A) was fitted by the same components. In addition, the weak peak at a binding energy of 291 eV is assigned to the C−F and/or Cl group.[62,63] In the F 1s region, the fitted peaks can be attributed to F−V, F_x−Ti−C, and F−C bonds in both samples (Figure 7B and 8B). In the $TiVCT_x$-HF sample the F−C bonds are centered at 686.5 eV and 688 eV, while in the $TiVCT_x$-LiF/HCl sample they are located at binding energies of 688.5 eV and 693 eV. We do not completely understand the reason for the large shifts of F−C binding energies in the $TiVCT_x$-LiF/HCl sample, but it might be related to the different carbon−fluorine interactions in the material. In general, covalent C−F bonds show higher binding energies than ionic bonds.[62] Figure 7C shows the Ti 2P spectrum of the $Ti_3C_2T_x$-HF sample. The three dominant peaks at 454.6, 455.8, and 458.2 eV correspond to Ti−C, Ti−O, and C−Ti−F_x bonds.[58,60] In the $Ti_3C_2T_x$-LiF/HCl sample, two new peaks emerged at 453 and 458 eV (Figure 8C), which are attributed to pure Ti and Ti−Cl bonds, respectively.[64,65]

Figures 7D and 8D show V 2p and O 1s spectra of the two samples. The V 2p region of the Ti_3C_2-HF sample is composed of four peaks. Peaks at 514 and 515.4 eV correspond to the different oxidation states of vanadium and the other two peaks at 513 and 518.4 eV are assigned to V−C and V−F.[66−68] In the V 2P region of Ti_3C_2-LiF/HCl, an additional peak is fitted at 514.7 eV, which can be attributed to V−Cl bonds.[69] In the O 1s region, three main peaks are assigned to O−Ti, V=O, and −OH bonds. The presence of water molecules between MXene flakes is also found in the O 1s regions of both samples.

The surface compositions of $TiVCT_x$ MXenes determined by XPS are reported in Table 2. It is shown that the amount of oxygen increased to ∼34 at. % in the $TiVCT_x$-LiF/HCl sample compared to ∼23 at. % in $TiVCT_x$-HF, while the fluorine concentration decreased from ∼20 at. % in $TiVCT_x$-HF to ∼12 at. % in the $TiVCT_x$-LiF/HCl sample. These results are in good agreement with the less precise EDS measurements shown earlier. A higher number of =O compared to other functional groups has been reported on other MXenes (e.g, $Ti_3C_2T_x$ and V_2CT_x), which were synthesized by a mixture of

https://dx.doi.org/10.1021/acsami.0c03181
ACS Appl. Mater. Interfaces 2020, 12, 20129−20137

fluoride salts and HCl as well.[26,70] XPS analysis also enables us to determine the −OH concentration, which is not possible with EDS. Compared to the =O and −F functional groups, −OH and −Cl are minor components on $TiVCT_x$ MXene (Tables 2, S3, and S4). Based on the XPS results, no significant effect of the −OH concentration has been observed on the $TiVCT_x$ MXene synthesized by two different solutions.

CONCLUSIONS

In summary, we systematically compared the effect of synthesis condition on the functional groups of 2D $TiVCT_x$ solid-solution MXenes. Large-scale delamination and separation of solid-solution MXene layers were achieved by treating the stacked MXenes (synthesized by LiF/HCl) with TBAOH at room temperature without a sonication step. Compared to the $TiVCT_x$-stacked MXene, a larger interlayer spacing was observed for the $TiVCT_x$ film (separated MXene flakes), suggesting intercalation of water molecules and/or TBA^+ ions between MXene layers. Based on DFT calculations, TiVC with the =O functional group has the most stable structure and also the =O functional group has more adhesion on the surface of TiVC MXenes compared to other terminations. EDS and XPS analyses show that using a mild etchant of LiF/HCl for the synthesis of $TiVCT_x$ results in an increase of =O and a decrease of −F terminations on the MXene relative to the common use of highly concentrated HF. XPS studies reveal that the synthesis condition has no significant effect on the −OH concentration of TiVC MXene. The utilization of the LiF/HCl solution is desirable for reducing the toxicity and causticity in the synthesis of MXenes, and our results also show that this solution provides a more favorable surface chemistry for energy-storage applications.

ASSOCIATED CONTENT

Supporting Information

The Supporting Information is available free of charge at https://pubs.acs.org/doi/10.1021/acsami.0c03181.

Rietveld refined XRD pattern of the as-synthesized MAX phase; XRD and SEM images of TiVC synthesized by 50% HF; three base structures with different transition-metal ion configurations of solid-solution TiVC MXenes; calculations of the cohesive energies and adsorption energies of different functional groups on TiVC MXenes; XPS peak fitting results of $TiVCT_x$ MXenes prepared by 50% HF and 1.9 M LiF/12 M HCl.(PDF)

AUTHOR INFORMATION

Corresponding Author

Sanaz Yazdanparast − *Department of Metallurgical and Materials Engineering, Colorado School of Mines, Golden, Colorado 80401, United States;* orcid.org/0000-0002-6135-9469; Email: syazdanparast@mines.edu

Authors

Sina Soltanmohammad − *Department of Metallurgical and Materials Engineering, Colorado School of Mines, Golden, Colorado 80401, United States*

Annika Fash-White − *Department of Mechanical Engineering, Colorado School of Mines, Golden, Colorado 80401, United States*

Garritt J. Tucker − *Department of Mechanical Engineering, Colorado School of Mines, Golden, Colorado 80401, United States*

Geoff L. Brennecka − *Department of Metallurgical and Materials Engineering, Colorado School of Mines, Golden, Colorado 80401, United States*

Complete contact information is available at: https://pubs.acs.org/10.1021/acsami.0c03181

Notes

The authors declare no competing financial interest.

ACKNOWLEDGMENTS

GB was partially supported by the National Science Foundation (DMR-1555015). AFW and GJT were partially supported by funding through the National Science Foundation (DMR1728041).

REFERENCES

(1) Chaudhari, N. K.; Jin, H.; Kim, B.; San Baek, D.; Joo, S. H.; Lee, K. MXene: An Emerging Two-Dimensional Material for Future Energy Conversion and Storage Applications. *J. Mater. Chem. A* **2017**, *5*, 24564−24579.

(2) Halim, J.; Lukatskaya, M. R.; Cook, K. M.; Lu, J.; Smith, C. R.; Näslund, L. Å.; May, S. J.; Hultman, L.; Gogotsi, Y.; Eklund, P.; Barsoum, M. W. Transparent Conductive Two-Dimensional Titanium Carbide Epitaxial Thin Films. *Chem. Mater.* **2014**, *26*, 2374−2381.

(3) Shahzad, F.; Alhabeb, M.; Hatter, C. B.; Anasori, B.; Hong, S. M.; Koo, C. M.; Gogotsi, Y. Electromagnetic Interference Shielding with 2D Transition Metal Carbides (MXenes). *Science* **2016**, *353*, 1137−1140.

(4) Barsoum, M. W. The MN+1AXN Phases: A New Class of Solids. *Prog. Solid State Chem.* **2000**, *28*, 201−281.

(5) Naguib, M.; Kurtoglu, M.; Presser, V.; Lu, J.; Niu, J.; Heon, M.; Hultman, L.; Gogotsi, Y.; Barsoum, M. W. Two-Dimensional Nanocrystals Produced by Exfoliation of Ti3AlC2. *Adv. Mater.* **2011**, *23*, 4248−4253.

(6) Naguib, M.; Mochalin, V. N.; Barsoum, M. W.; Gogotsi, Y. 25th Anniversary Article: MXenes: A New Family of Two-Dimensional Materials. *Adv. Mater.* **2014**, *26*, 992−1005.

(7) Luo, J.; Zhang, W.; Yuan, H.; Jin, C.; Zhang, L.; Huang, H.; Liang, C.; Xia, Y.; Zhang, J.; Gan, Y.; Tao, X. Pillared Structure Design of MXene with Ultralarge Interlayer Spacing for High-Performance Lithium-Ion Capacitors. *ACS Nano* **2017**, *11*, 2459−2469.

(8) Plummer, G.; Anasori, B.; Gogotsi, Y.; Tucker, G. J. Nanoindentation of Monolayer Tin+1CnTx MXenes via Atomistic Simulations: The Role of Composition and Defects on Strength. *Comput. Mater. Sci.* **2019**, *157*, 168−174.

(9) Zhang, N.; Hong, Y.; Yazdanparast, S.; Asle Zaeem, M. Superior Structural, Elastic and Electronic Properties of 2D Titanium Nitride MXenes over Carbide MXenes: A Comprehensive First Principles Study. *2D Mater.* **2018**, *5*, No. 045004.

(10) Naguib, M.; Mashtalir, O.; Carle, J.; Presser, V.; Lu, J.; Hultman, L.; Gogotsi, Y.; Barsoum, M. W. Two-Dimensional Transition Metal Carbides. *ACS Nano* **2012**, *6*, 1322−1331.

(11) Naguib, M.; Halim, J.; Lu, J.; Cook, K.; Hultman, L.; Gogotsi, Y.; Barsoum, M. W. New Two-Dimensional Niobium and Vanadium Carbides as Promising Materials for Li-Ion Batteries. *J. Am. Chem. Soc.* **2013**, *135*, 15966−15969.

(12) Simon, P. Two-Dimensional MXene with Controlled Interlayer Spacing for Electrochemical Energy Storage. *ACS Nano* **2017**, *11*, 2393−2396.

(13) Peng, Q.; Guo, J.; Zhang, Q.; Xiang, J.; Liu, B.; Zhou, A.; Liu, R.; Tian, Y. Unique Lead Adsorption Behavior of Activated Hydroxyl Group in Two-Dimensional Titanium Carbide. *J. Am. Chem. Soc.* **2014**, *136*, 4113−4116.

(14) Zhang, Q.; Teng, J.; Zou, G.; Peng, Q.; Du, Q.; Jiao, T.; Xiang, J. Efficient Phosphate Sequestration for Water Purification by Unique Sandwich-like MXene/Magnetic Iron Oxide Nanocomposites. *Nanoscale* **2016**, *8*, 7085−7093.
(15) Jiang, X.; Liu, S.; Liang, W.; Luo, S.; He, Z.; Ge, Y.; Wang, H.; Cao, R.; Zhang, F.; Wen, Q.; Li, J.; Bao, Q.; Fan, D.; Zhang, H. Broadband Nonlinear Photonics in Few-Layer MXene Ti3C2Tx (T = F, O, or OH). *Laser Photonics Rev.* **2018**, *12*, No. 1700229.
(16) Lin, H.; Wang, X.; Yu, L.; Chen, Y.; Shi, J. Two-Dimensional Ultrathin MXene Ceramic Nanosheets for Photothermal Conversion. *Nano Lett.* **2017**, *17*, 384−391.
(17) Ghidiu, M.; Lukatskaya, M. R.; Zhao, M. Q.; Gogotsi, Y.; Barsoum, M. W. Conductive Two-Dimensional Titanium Carbide "clay" with High Volumetric Capacitance. *Nature* **2014**, *516*, 78−81.
(18) Li, H.; Hou, Y.; Wang, F.; Lohe, M. R.; Zhuang, X.; Niu, L.; Feng, X. Flexible All-Solid-State Supercapacitors with High Volumetric Capacitances Boosted by Solution Processable MXene and Electrochemically Exfoliated Graphene. *Adv. Energy Mater.* **2017**, *7*, No. 1601847.
(19) Xie, Y.; Naguib, M.; Mochalin, V. N.; Barsoum, M. W.; Gogotsi, Y.; Yu, X.; Nam, K. W.; Yang, X. Q.; Kolesnikov, A. I.; Kent, P. R. C. Role of Surface Structure on Li-Ion Energy Storage Capacity of Two-Dimensional Transition-Metal Carbides. *J. Am. Chem. Soc.* **2014**, *136*, 6385−6394.
(20) Li, J.; Yuan, X.; Lin, C.; Yang, Y.; Xu, L.; Du, X.; Xie, J.; Lin, J.; Sun, J. Achieving High Pseudocapacitance of 2D Titanium Carbide (MXene) by Cation Intercalation and Surface Modification. *Adv. Energy Mater.* **2017**, *7*, No. 1602725.
(21) Luo, J.; Fang, C.; Jin, C.; Yuan, H.; Sheng, O.; Fang, R.; Zhang, W.; Huang, H.; Gan, Y.; Xia, Y.; Liang, C.; Zhang, J.; Li, W.; Tao, X. Tunable pseudocapacitance storage of MXene by cation pillaring for high performane sodium-ion capacitors. *J. Mater. Chem. A* **2018**, *6*, 7794−7806.
(22) Lukatskaya, M. R.; Bak, S. M.; Yu, X.; Yang, X. Q.; Barsoum, M. W.; Gogotsi, Y. Probing the Mechanism of High Capacitance in 2D Titanium Carbide Using in Situ X-Ray Absorption Spectroscopy. *Adv. Energy Mater.* **2015**, *5*, No. 1500589.
(23) Dall'Agnese, Y.; Lukatskaya, M. R.; Cook, K. M.; Taberna, P. L.; Gogotsi, Y.; Simon, P. High Capacitance of Surface-Modified 2D Titanium Carbide in Acidic Electrolyte. *Electrochem. Commun.* **2014**, *48*, 118−122.
(24) Tang, Q.; Zhou, Z.; Shen, P. Are MXenes Promising Anode Materials for Li Ion Batteries? Computational Studies on Electronic Properties and Li Storage Capability of Ti3C2 and Ti3C2X2 (X = F, OH) Monolayer. *J. Am. Chem. Soc.* **2012**, *134*, 16909−16916.
(25) Fang, R.; Lu, C.; Chen, A.; Wang, K.; Huang, H.; Gan, Y.; Liang, C.; Zhang, J.; Tao, X.; Xia, Y.; Zhang, W. 2D MXene-based Energy Storage Materials: Interfacial Structure Design and Functionalization. *ChemSusChem* **2019**, *12*, 1−12.
(26) Hope, M. A.; Forse, A. C.; Griffith, K. J.; Lukatskaya, M. R.; Ghidiu, M.; Gogotsi, Y.; Grey, C. P. NMR Reveals the Surface Functionalisation of Ti3C2 MXene. *Phys. Chem. Chem. Phys.* **2016**, *18*, 5099−5102.
(27) Anasori, B.; Xie, Y.; Beidaghi, M.; Lu, J.; Hosler, B. C.; Hultman, L.; Kent, P. R. C.; Gogotsi, Y.; Barsoum, M. W. Two-Dimensional, Ordered, Double Transition Metals Carbides (MXenes). *ACS Nano* **2015**, *9*, 9507−9516.
(28) Anasori, B.; Lukatskaya, M. R.; Gogotsi, Y. 2D Metal Carbides and Nitrides (MXenes) for Energy Storage. *Nat. Rev. Mater.* **2017**, *2*, No. 16098.
(29) Liu, F.; Zhou, A.; Chen, J.; Jia, J.; Zhou, W.; Wang, L.; Hu, Q. Preparation of Ti3C2 and Ti2C MXenes by Fluoride Salts Etching and Methane Adsorptive Properties. *Appl. Surf. Sci.* **2017**, *416*, 781−789.
(30) Halim, J.; Kota, S.; Lukatskaya, M. R.; Naguib, M.; Zhao, M. Q.; Moon, E. J.; Pitock, J.; Nanda, J.; May, S. J.; Gogotsi, Y.; Barsoum, M. W. Synthesis and Characterization of 2D Molybdenum Carbide (MXene). *Adv. Funct. Mater.* **2016**, *26*, 3118−3127.
(31) Mashtalir, O.; Lukatskaya, M. R.; Zhao, M. Q.; Barsoum, M. W.; Gogotsi, Y. Amine-Assisted Delamination of Nb2C MXene for Li-Ion Energy Storage Devices. *Adv. Mater.* **2015**, *27*, 3501−3506.
(32) Naguib, M.; Unocic, R. R.; Armstrong, B. L.; Nanda, J. Large-Scale Delamination of Multi-Layers Transition Metal Carbides and Carbonitrides "MXenes.". *Dalton Trans.* **2015**, *44*, 9353−9358.
(33) Soundiraraju, B.; George, B. K. Two-Dimensional Titanium Nitride (Ti2N) MXene: Synthesis, Characterization, and Potential Application as Surface-Enhanced Raman Scattering Substrate. *ACS Nano* **2017**, *11*, 8892−8900.
(34) Wong, Z. M.; Tan, T. L.; Yang, S. W.; Xu, G. Q. Enhancing the Photocatalytic Performance of MXenes via Stoichiometry Engineering of Their Electronic and Optical Properties. *ACS Appl. Mater. Interfaces* **2018**, *10*, 39879−39889.
(35) Hu, Y.; Fan, X. L.; Guo, W. J.; An, Y. R.; Luo, Z. F.; Kong, J. Ordered Double-M Elements MXenes TiMC: Large in-Plane Stiffness and Ferromagnetism. *J. Magn. Magn. Mater.* **2019**, *486*, No. 165280.
(36) Mashtalir, O.; Naguib, M.; Mochalin, V. N.; Dall'Agnese, Y.; Heon, M.; Barsoum, M. W.; Gogotsi, Y. Intercalation and Delamination of Layered Carbides and Carbonitrides. *Nat. Commun.* **2013**, *4*, No. 1716.
(37) Wang, Y.; Zheng, W.; Zhang, P.; Tian, W.; Chen, J.; Sun, Z. M. Preparation of (Vx, Ti1−x)2C MXenes and Their Performance as Anode Materials for LIBs. *J. Mater. Sci.* **2019**, *54*, 11991−11999.
(38) Kent, P. R. C.; Alhabeb, M.; Van Aken, K. L.; Gogotsi, Y.; Unocic, R. R.; Xie, Y.; Lin, M.-W.; Xiao, K.; Sang, X. Atomic Defects in Monolayer Titanium Carbide (Ti3C2Tx) MXene. *ACS Nano* **2016**, *10*, 9193−9200.
(39) Alhabeb, M.; Maleski, K.; Anasori, B.; Lelyukh, P.; Clark, L.; Sin, S.; Gogotsi, Y. Guidelines for Synthesis and Processing of Two-Dimensional Titanium Carbide (Ti3C2Tx MXene). *Chem. Mater.* **2017**, *29*, 7633−7644.
(40) Naguib, M. MXenes: A New Family of Two-Dimensional Materials and Its Application as Electrodes for Li-Ion Batteries. Ph.D. Thesis, Drexel University, 2014.
(41) ICDD.*PDF-4+ 2020 (Database)*; International Centre for Diffraction Data: Newtown Square, PA, 2020.
(42) Kresse, G.; Furthmüller, J. Efficient Iterative Schemes for Ab Initio Total-Energy Calculations Using a Plane-Wave Basis Set. *Phys. Rev. B - Condens. Matter Mater. Phys.* **1996**, *54*, 11169−11186.
(43) Kresse, G.; Hafner, J. Ab Initio Molecular-Dynamics Simulation of the Liquid-Metalamorphous- Semiconductor Transition in Germanium. *Phys. Rev. B* **1994**, *49*, 14251−14269.
(44) Kresse, G. Ab Initio Molecular Dynamics for Liquid Metals. *J. Non-Cryst. Solids* **1995**, *192*−*193*, 222−229.
(45) Kresse, G.; Furthmüller, J. Efficiency of Ab-Initio Total Energy Calculations for Metals and Semiconductors Using a Plane-Wave Basis Set. *Comput. Mater. Sci.* **1996**, *6*, 15−50.
(46) Blöchl, P. E. Projector Augmented-Wave Method. *Phys. Rev. B* **1994**, *50*, 17953−17979.
(47) Perdew, J. P.; Burke, K.; Ernzerhof, M. Generalized Gradient Approximation Made Simple. *Phys. Rev. Lett.* **1996**, *77*, 3865−3868.
(48) Zhang, C. J.; Pinilla, K. S.; McEvoy, N.; Cullen, C. P.; Anasori, B.; Long, E.; Park, S.-H.; Seral-Ascaso, A.; Shmeliov, A.; Krishnan, D.; Morant, C.; Liu, X.; Duesberg, G. S.; Gogotsi, Y.; Nicolosi, V. Oxidation Stability of Colloidal Two-Dimensional Titanium Carbide (MXenes). *Chem. Mater.* **2017**, *29*, 4848−4856.
(49) Dall'Agnese, Y.; Taberna, P. L.; Gogotsi, Y.; Simon, P. Two-Dimensional Vanadium Carbide (MXene) as Positive Electrode for Sodium-Ion Capacitors. *J. Phys. Chem. Lett.* **2015**, *6*, 2305−2309.
(50) Dong, Y.; Chertopalov, S.; Maleski, K.; Anasori, B.; Hu, L.; Bhattacharya, S.; Rao, A. M.; Gogotsi, Y.; Mochalin, V. N.; Podila, R. Saturable Absorption in 2D Ti3C2 MXene Thin Films for Passive Photonic Diodes. *Adv. Mater.* **2018**, *30*, No. 1705714.
(51) Huang, K.; Li, Z.; Lin, J.; Han, G.; Huang, P. Two-Dimensional Transition Metal Carbides and Nitrides (MXenes) for Biomedical Applications. *Chem. Soc. Rev.* **2018**, *47*, 5109−5124.
(52) Ren, C. E.; Hatzell, K. B.; Alhabeb, M.; Ling, Z.; Mahmoud, K. A.; Gogotsi, Y. Charge- and Size-Selective Ion Sieving Through

https://dx.doi.org/10.1021/acsami.0c03181
ACS Appl. Mater. Interfaces 2020, 12, 20129−20137

Ti3C2Tx MXene Membranes. *J. Phys. Chem. Lett.* **2015**, *6*, 4026−4031.
(53) Verger, L.; Natu, V.; Ghidiu, M.; Barsoum, M. W. Effect of Cationic Exchange on the Hydration and Swelling Behavior of Ti3C2Tz MXenes. *J. Phys. Chem. C* **2019**, *123*, 20044−20050.
(54) Zhang, T.; Pan, L.; Tang, H.; Du, F.; Guo, Y.; Qiu, T.; Yang, J. Synthesis of Two-Dimensional Ti3C2Tx MXene Using HCl+LiF Etchant: Enhanced Exfoliation and Delamination. *J. Alloys Compd.* **2017**, *695*, 818−826.
(55) Khazaei, M.; Arai, M.; Sasaki, T.; Chung, C. Y.; Venkataramanan, N. S.; Estili, M.; Sakka, Y.; Kawazoe, Y. Novel Electronic and Magnetic Properties of Two-Dimensional Transition Metal Carbides and Nitrides. *Adv. Funct. Mater.* **2013**, *23*, 2185−2192.
(56) Kumar, S.; Lei, Y.; Alshareef, N. H.; Quevedo-Lopez, M. A.; Salama, K. N. Biofunctionalized Two-Dimensional Ti3C2 MXenes for Ultrasensitive Detection of Cancer Biomarker. *Biosens. Bioelectron.* **2018**, *121*, 243−249.
(57) Antonik, M. D.; Lad, R. J.; Christensen, T. M. Clean Surface and Oxidation Behavior of Vanadium Carbide, VC0.75(100). *Surf. Interface Anal.* **1996**, *24*, 681−686.
(58) Halim, J.; Cook, K. M.; Naguib, M.; Eklund, P.; Gogotsi, Y.; Rosen, J.; Barsoum, M. W. X-Ray Photoelectron Spectroscopy of Select Multi-Layered Transition Metal Carbides (MXenes). *Appl. Surf. Sci.* **2016**, *362*, 406−417.
(59) Jayaweera, P. M.; Quah, E. L.; Idriss, H. Photoreaction of Ethanol on TiO2(110) Single-Crystal Surface. *J. Phys. Chem. C* **2007**, *111*, 1764−1769.
(60) Kong, F.; He, X.; Liu, Q.; Qi, X.; Zheng, Y.; Wang, R.; Bai, Y. Improving the Electrochemical Properties of MXene Ti3C2 Multi-layer for Li-Ion Batteries by Vacuum Calcination. *Electrochim. Acta* **2018**, *265*, 140−150.
(61) Han, M.; Yin, X.; Wu, H.; Hou, Z.; Song, C.; Li, X.; Zhang, L.; Cheng, L. Ti3C2 MXenes with Modified Surface for High-Performance Electromagnetic Absorption and Shielding in the X-Band. *ACS Appl. Mater. Interfaces* **2016**, *8*, 21011−21019.
(62) Kang, W.; Li, S. Preparation of Fluorinated Graphene to Study Its Gas Sensitivity. *RSC Adv.* **2018**, *8*, 23459−23467.
(63) Lindberg, B. J.; Hamrin, K.; Johansson, G.; Gelius, U.; Fahlman, A.; Nordling, C.; Siegbahn, K.; Nordberg, R. Molecular Spectroscopy by Means of Esca. *Phys. Scr.* **1970**, *2*, 70−80.
(64) Anderson, C. R.; Lee, R. N.; Morar, J. F.; Park, R. L. Comparison of Aps and Fresca Core Level Binding Energy Measurements. *J. Vac. Sci. Technol.* **1982**, *20*, 617−621.
(65) Mousty-Desbuquoit, C.; Riga, J.; Verbist, J. J. Solid State Effects in the Electronic Structure of TiCl4 Studied by XPS. *J. Chem. Phys.* **1983**, *79*, 26−32.
(66) Colton, R. J.; Guzman, A. M.; Rabalais, J. W. Electrochromism in Some Thin-Film Transition-Metal Oxides Characterized by X-Ray Electron Spectroscopy. *J. Appl. Phys.* **1978**, *49*, 409−416.
(67) Groenenboom, C. J.; Sawatzky, G.; de Liefde Meijer, H. J.; Jellinek, F. Electron Spectroscopy of Some Cyclopentadienylcyclo-heptatrienylmetal Compounds. *J. Organomet. Chem.* **1974**, *76*, C4−C6.
(68) Groult, H.; Devilliers, D.; Kumagai, N.; Nakajima, T.; Matsuo, Y. Vanadium Oxide Fluoride-Graphite Intercalation Compounds: Structural Characteristics and Electrochemical Insertion of Lithium Cations. *J. Electrochem. Soc.* **1996**, *143*, 2093−2099.
(69) Horvath, B.; Strutz, J.; Geyer-Lippmann, J.; Horvath, E. G. Preparation, Properties, and ESCA Characterization of Vanadium Surface Compounds on Silicagel.II. *Z. Anorg. Allg. Chem.* **1981**, *483*, 181−192.
(70) Liu, F.; Zhou, J.; Wang, S.; Wang, B.; Shen, C.; Wang, L.; Hu, Q.; Huang, Q.; Zhou, A. Properties of High-Purity V_2C MXene and Electrochemical Properties as Li-Ion Batteries. *J. Electrochem. Soc.* **2017**, *164*, A709−A713.

https://dx.doi.org/10.1021/acsami.0c03181
ACS Appl. Mater. Interfaces 2020, 12, 20129−20137